

## Broad-band nonlinear optical response in $\text{Bi}_2\text{Te}_{0.6}\text{S}_{2.4}$ alloys based on the Alloying-engineered

Haixia Zhu<sup>1</sup>, Zhaozhe Chen<sup>1</sup>, Rui Dai<sup>1</sup>, Bojun Yang<sup>1</sup>, Mianzeng Zhong<sup>1</sup>, Si Xiao<sup>1</sup>, Jun He<sup>1</sup>

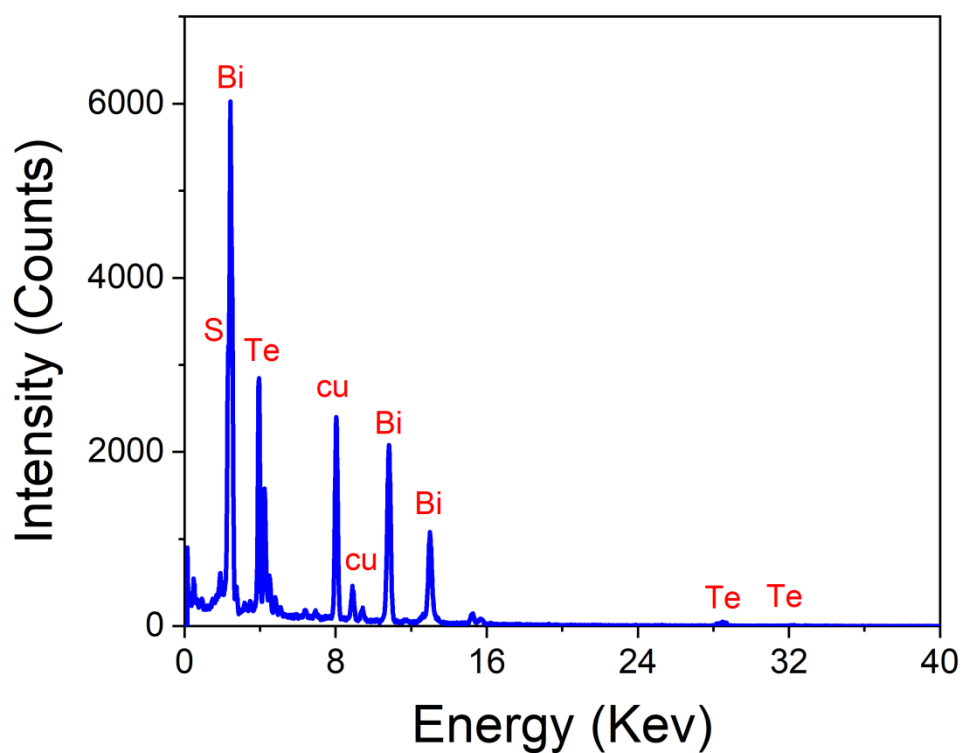


Figure S1. Energy-dispersive X-ray spectroscopy (EDS) spectrum of  $\text{Bi}_2(\text{Te}_x\text{Se}_{1-x})_3$  crystals.

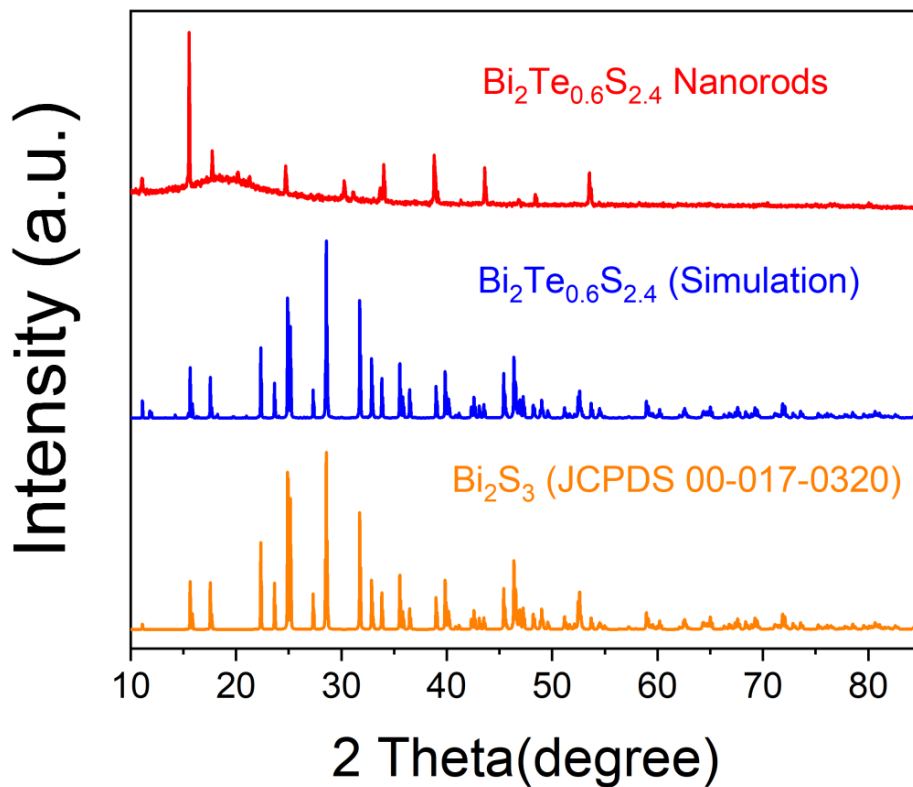


Figure S2. XRD pattern of  $\text{Bi}_2\text{Te}_{0.6}\text{S}_{2.4}$  nanorods (top), simulation  $\text{Bi}_2\text{Te}_{0.6}\text{S}_{2.4}$  powder (middle), and JCPDS 00-017-0320 ( $\text{Bi}_2\text{S}_3$ ) (bottom).

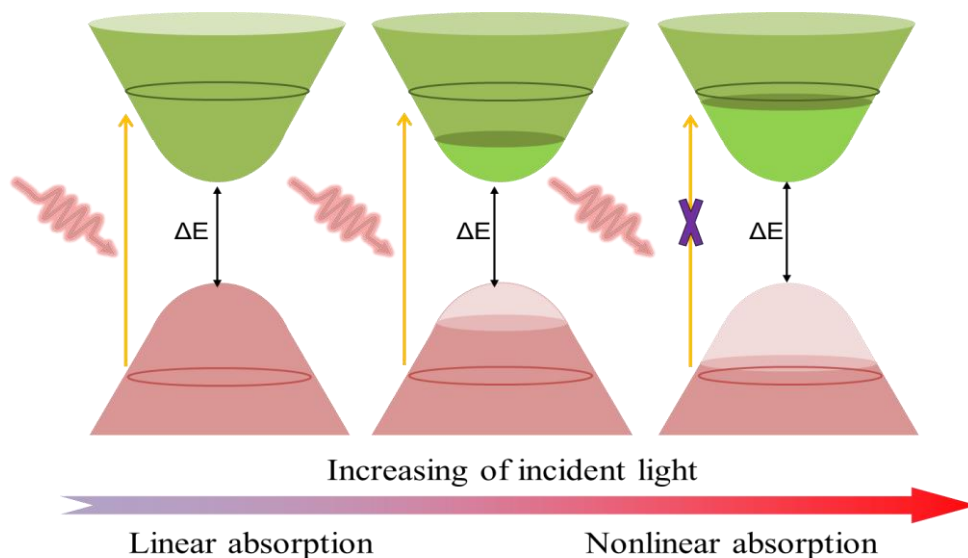


Figure S3 Schematic diagram of saturable absorption due to Pauli blocking principle.

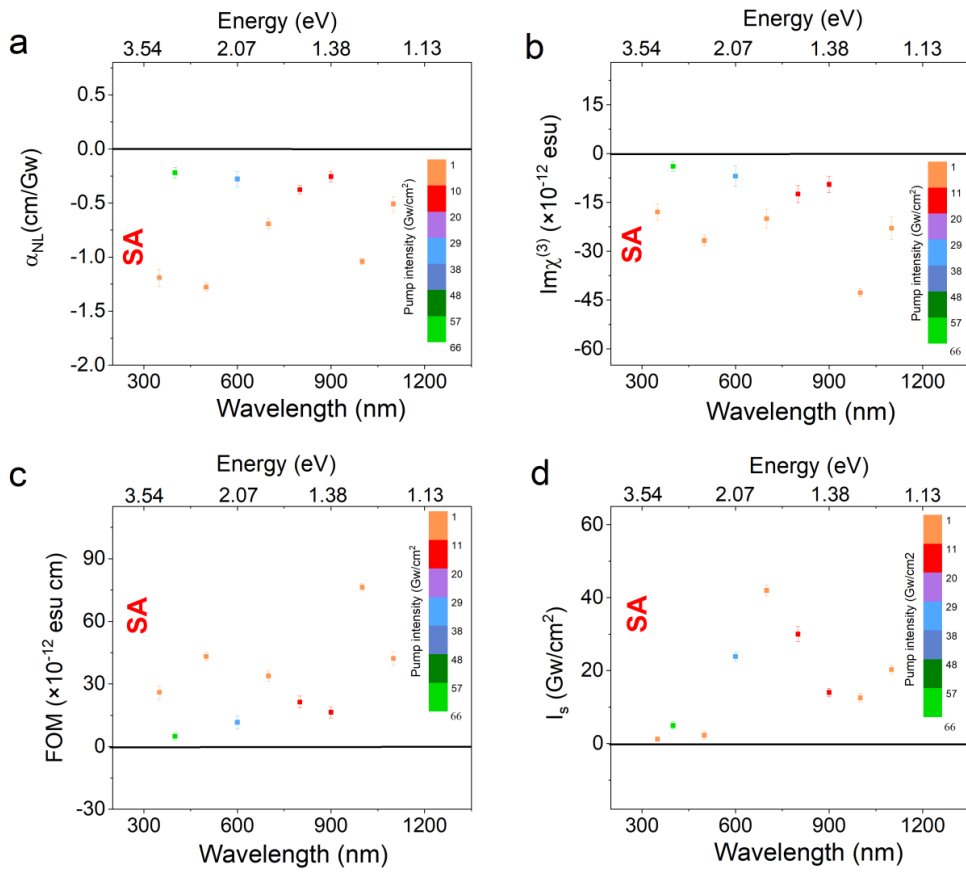


Figure S4 Wavelength dependence of (a) nonlinear absorption coefficient (b) the imaginary part of the third-order nonlinear optical susceptibility (c) the figure of merit (d) saturable absorption intensity.

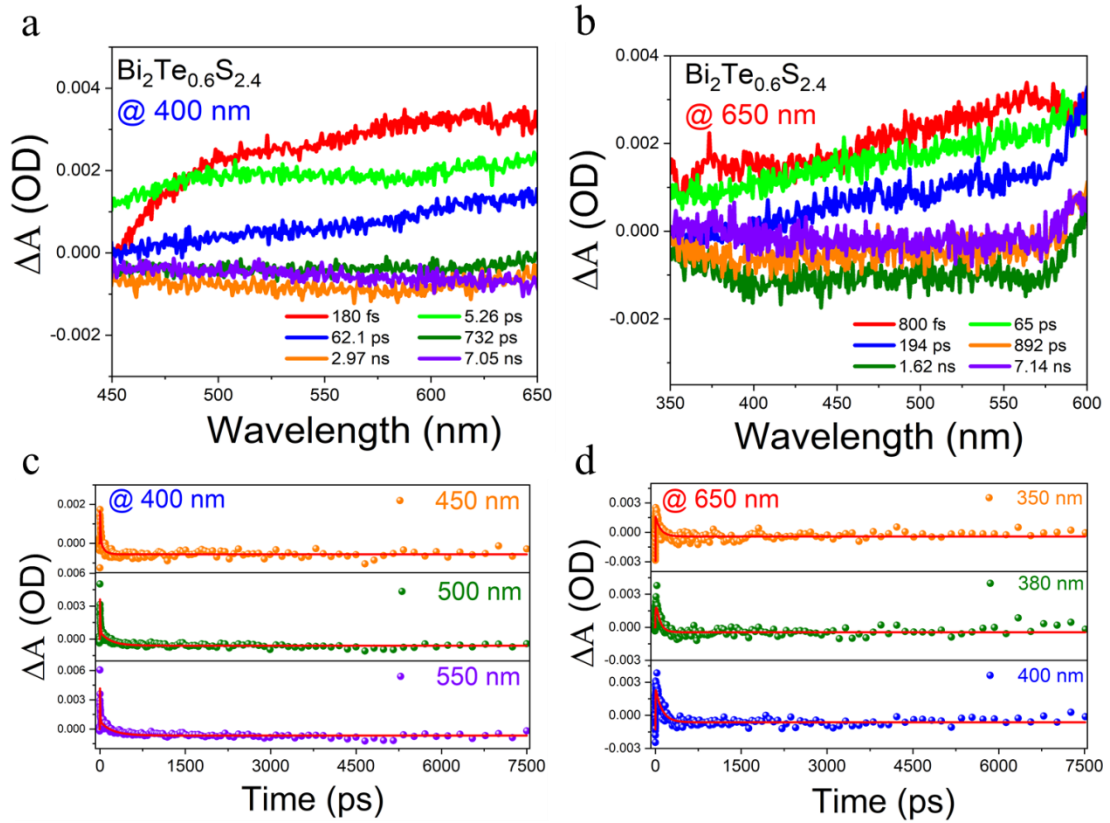


Figure S5 fs transient absorption spectra of  $\text{Bi}_2\text{Te}_{0.6}\text{S}_{2.4}$  nanorods pumped at 400 nm (a) and 650 nm (b). Dynamic curves and fitted results of  $\text{Bi}_2\text{Te}_{0.6}\text{S}_{2.4}$  nanorods pumped at 400 nm (c) and 650 nm (d).

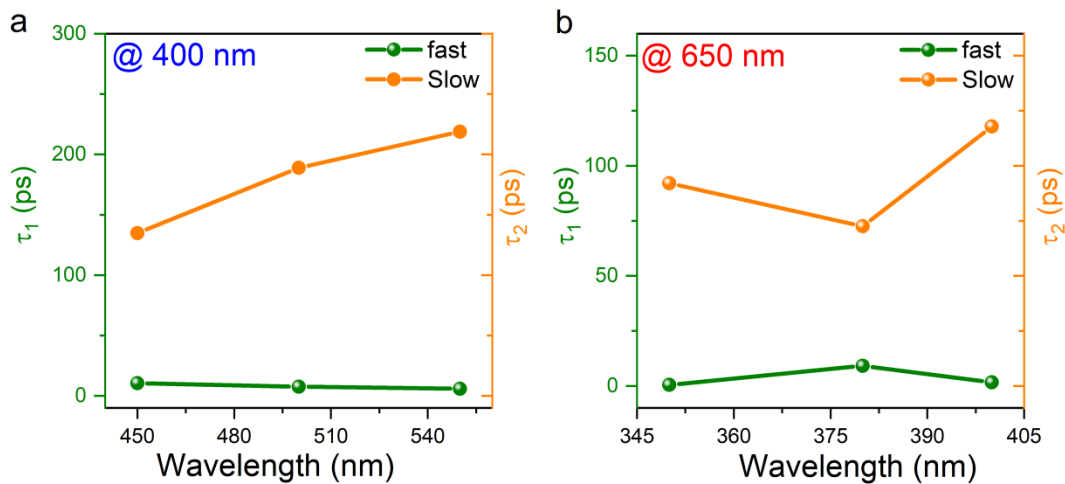


Figure S6 Fitting results of two ultrafast relaxation times pumped at 400 nm (a) and 650 nm (b), respectively.